Journal of Engineering Mathematics 22: 3–13 (1988)

Critical free-surface flow over a semi-circular obstruction

L.K. FORBES
Department of Mathematics, University of Queensland, St. Lucia 4067, Queensland, Australia

Received 9 April 1987; accepted in revised form 8 September 1987

Abstract. Numerical solutions are presented for the problem of two-dimensional "critical" flow of an ideal fluid over a semi-circular obstacle attached to the bottom of a running stream. The upstream Froude number and downstream flow speed are unknown in advance, and are therefore computed as part of the solution. The dependence of flow behaviour on obstacle size is discussed.

1. Introduction

The description of steady, two-dimensional flow of an ideal fluid in an open channel is a basic problem in fluid mechanics and hydraulics, and is discussed frequently in the literature. The essential features of such flows, in the presence of an obstruction in the channel, are given by Lamb [5]. According to linearized theory, in which the size of the disturbing obstacle is assumed to be small, the flow takes one of two possible forms, depending on the value of the upstream Froude number F, which is the ratio of the phase speed of the fluid infinitely far upstream to the speed at which a small disturbance would travel in the fluid. If $F < 1$, linearized theory predicts a region of uniform flow far ahead of the obstruction, followed by a train of downstream waves. When $F > 1$, a wave-free solution is obtained, in which the fluid surface simply rises over the obstacle, before returning to the undisturbed level downstream. There is no linearized solution when $F = 1$.

Forbes and Schwartz [4] used a boundary-integral technique to obtain numerical solutions to the exact, non-linear equations governing the flow of an ideal fluid in a channel with a semi-circular obstruction on the bottom. They found that the non-linear results were generally qualitatively similar to the predictions of linearized theory, with a train of downstream waves produced when $F < 1$, and a wave-free symmetric surface profile when $F > 1$. Their results, however, are inconclusive near $F = 1$, and in fact they conjectured that solutions possessing waves might also be possible in the approximate interval $1 \lesssim F \lesssim 1.3$, giving possible non-uniqueness of solutions for these values of F. Their argument was based on the assumption that, as F increased, the wavelength of the downstream waves would increase, ultimately giving a downstream solitary wave at about $F \approx 1.3$.

Recent work by Vanden-Broeck [9] casts some doubt on the validity of the above conjecture. He finds that non-uniqueness of solutions is indeed a possibility when $F > 1$, with one type of solution corresponding to perturbation of uniform flow, and the other type representing a perturbed solitary wave, similar to the conjecture of Forbes and Schwartz [4]. However, Vanden-Broeck's solitary-wave solutions do *not* emanate from the sub-critical ($F < 1$) region, are symmetric about the semi-circle and do *not* possess waves.

Non-uniqueness of solutions is also a possibility when $F < 1$. In addition to the solutions possessing downstream waves, there is another well-known solution type, referred to as

"critical flow". In this case, there is a uniform sub-critical ($F < 1$) stream ahead of the obstacle, followed by a uniform super-critical ($F > 1$) stream behind the obstacle. Thus the flow resembles the cascade of fluid over a waterfall, and does not possess waves.

The computation of critical flow as a solution to the full non-linear equations of motion has been addressed by various authors. Aitchison [1] used a variable finite-element method to obtain flow over a bottom-mounted triangular weir, and a similar approach was used by Bettess and Bettess [2]. Both papers have the disadvantage that the upstream "radiation" condition is not specified in advance. Critical flow has also been obtained as a solution to equations derived from certain shallow-water theories, as is the case in the studies undertaken by Naghdi and Vongsarnpigoon [7], and Sivakumaran, Tingsanchali and Hosking [8]. This latter paper contains photographs of critical flow generated in a laboratory flume.

In the present paper, we solve the exact equations of two-dimensional ideal fluid flow over a semi-circular obstruction, using the formulation of Forbes and Schwartz [4]. Critical flow is obtained by allowing the upstream Froude number F to be sought as part of the solution, and specifying uniform flow upstream and downstream of the obstacle, with unknown depth and flow speed infinitely far downstream. Accurate numerical solutions are obtained for most Froude numbers, except in the low-speed limit $F \to 0$, when the flow downstream evidently becomes a thin fluid jet moving at high speed.

2. Formulation

Consider a semi-circular cylinder of radius R mounted on the bed of a horizontal channel. A cartesian coordinate system is defined, with the origin at the centre of the semi-circle and the y-axis pointing vertically. Fluid flows through the channel in the positive x-direction, with speed c and depth H infinitely far upstream. Relative to the coordinate axes the flow is steady and is subject to the acceleration g of gravity in the negative y-direction. Suppose that the flow is critical, with unknown uniform speed cV far downstream; then, by conservation of mass, the unknown downstream fluid depth is H/V.

The problem is now non-dimensionalized using H and c as reference length and speed, respectively. For ideal flow, there are then three relevant dimensionless parameters. These are the dimensionless downstream speed V, the circle radius

$$\alpha = \frac{R}{H}$$

and the depth-based Froude number

$$F = \frac{c}{(gH)^{1/2}}.$$

For critical flow, however, only one of these quantities can be specified independently. A sketch of the flow in dimensionless coordinates is given in Fig. 1.

Since the flow is irrotational and the fluid incompressible, a velocity potential ϕ and streamfunction ψ exist, in terms of which the horizontal and vertical components, u and v,

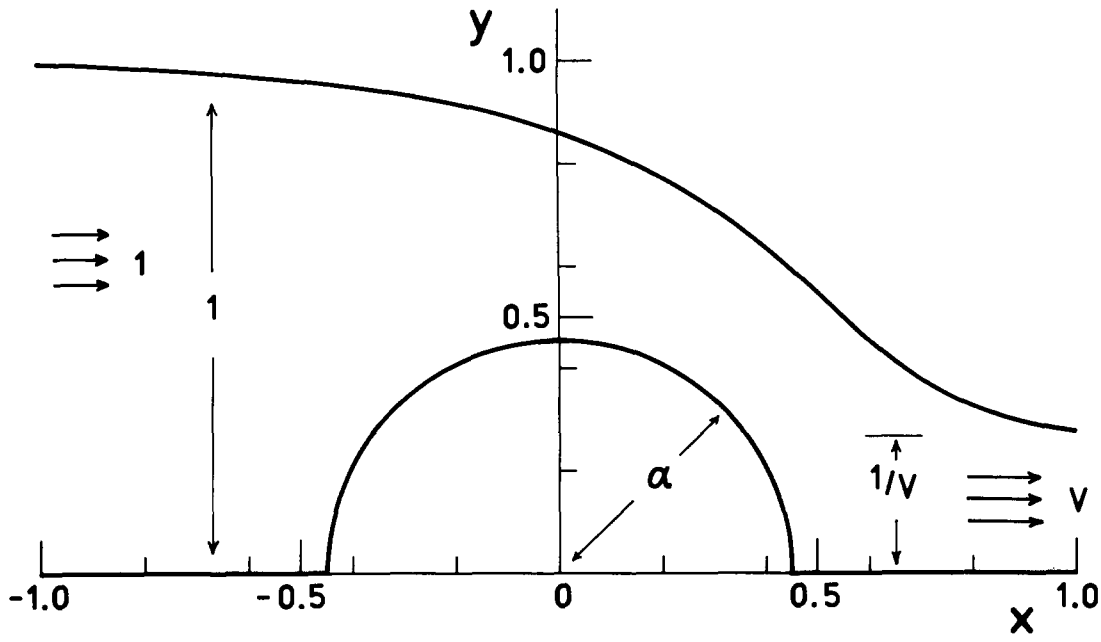

Fig. 1. Dimensionless flow configuration in the $z = x + iy$ plane. The free surface is a portion of an actual solution profile, obtained with $\alpha = 0.45$.

of the fluid velocity vector may be expressed as

$$u = \phi_x = \psi_y, \quad v = \phi_y = -\psi_x. \tag{2.1}$$

There is no component of flow normal to the bottom $y = h(x)$, where the bottom shape is defined by the function

$$h(x) = \begin{cases} (\alpha^2 - x^2)^{1/2}, & |x| \leqq \alpha \\ 0, & |x| \geqq \alpha \end{cases} \tag{2.2}$$

and the constant pressure condition at the fluid surface gives Bernoulli's equation in the form

$$\tfrac{1}{2}F^2(u^2 + v^2) + y = \tfrac{1}{2}F^2 + 1 \tag{2.3}$$

on the free surface.

For critical flow, the unknown downstream velocity is V in the positive x-direction, and the stream depth is $1/V$, as in Fig. 1. The Bernoulli equation (2.3) therefore gives a relation between V and the upstream Froude number F, of the form

$$F = \left[\frac{2}{V(V+1)}\right]^{1/2}. \tag{2.4}$$

The *downstream* Froude number is

$$F_{DS} = FV^{3/2}, \tag{2.5}$$

and thus, for $V > 1$, it necessarily follows from equations (2.4) and (2.5) that $F < 1$ upstream, whilst $F_{DS} > 1$ downstream.

Equations (2.1) show that the complex potential $f = \phi + \mathrm{i}\psi$ can be expressed as an analytic function of the variable $z = x + \mathrm{i}y$. Following Forbes and Schwartz [4], the z-plane is now mapped into a ζ-plane in which the bottom profile given in (2.2) becomes a straight line. The required mapping is

$$\zeta = \frac{1}{2}\left(z + \frac{\alpha^2}{z}\right),$$

which, upon solving for $z = x + \mathrm{i}y$ in terms of the new variable $\zeta = \xi + \mathrm{i}\eta$, yields

$$z = \zeta + (\zeta^2 - \alpha^2)^{1/2}. \tag{2.6}$$

Finally, the rôles of the variables f and ζ are interchanged, so that ζ is sought as an analytic function of f. This transformation has the advantage of simplifying the problem formulation to the extent that the bottom and the free surface map to the streamlines $\psi = 0$ and $\psi = 1$, respectively, in the f-plane.

The final form of the Bernoulli equation in the f-plane is

$$\frac{F^2(z^2 - \alpha^2)(\bar{z}^2 - \alpha^2)}{8(z\bar{z})^2(\xi_\phi^2 + \eta_\phi^2)} + y = \tfrac{1}{2}F^2 + 1 \quad \text{on} \quad \psi = 1, \tag{2.7}$$

where z is found from ζ using equation (2.6), and the bars denote complex conjugation. Forbes and Schwartz [4] have derived an integral equation relating the real and imaginary parts of the function $\mathrm{d}\zeta/\mathrm{d}f$ at the surface $\psi = 1$. This equation is

$$[\xi_\phi(\phi, 1) - \tfrac{1}{2}] - \frac{2}{\pi}\int_{-\infty}^{\infty} [\xi_\theta(\theta, 1) - \tfrac{1}{2}] \frac{\mathrm{d}\theta}{(\theta - \phi)^2 + 4}$$

$$= -\frac{1}{\pi}\int_{-\infty}^{\infty} \eta_\theta(\theta, 1) \left\{\frac{1}{\theta - \phi} + \frac{(\theta - \phi)}{(\theta - \phi)^2 + 4}\right\} \mathrm{d}\theta, \tag{2.8}$$

and automatically satisfies the bottom condition and the equations within the fluid. The integral on the right-hand side of (2.8) is singular in the Cauchy principal-value sense when $\theta = \phi$.

The free-surface profile for critical flow is thus obtained by solving equations (2.7) and (2.8) subject to (2.4) and the requirements

$$\zeta \to \tfrac{1}{2}f \quad \text{as} \quad \phi \to -\infty \tag{2.9}$$

and

$$\zeta \to \frac{1}{2V}f \quad \text{as} \quad \phi \to \infty, \tag{2.10}$$

giving conditions far upstream and far downstream of the semi-circle, respectively. Once ζ has been obtained at the free surface $\psi = 1$, its shape z can be obtained from equation (2.6).

3. Numerical methods

This problem is solved in essentially the same manner as that discussed by Forbes and Schwartz [4]. The free surface is truncated to some finite interval $\phi_1 \leqq \phi \leqq \phi_N$, and a grid of equally-spaced points ϕ_i, $i = 1, \ldots, N$ defined, according to

$$\phi_i = \phi_1 + (i - 1)h,$$

where the point spacing is

$$h = \frac{\phi_N - \phi_1}{N - 1}.$$

Newton's method is used to solve this problem for the vector of unknowns $\mathbf{u} = [\eta_2', \ldots, \eta_N']$. As an initial guess, we approximate the function $\eta_\phi(\phi, 1)$ at the free surface by the relationship

$$\eta_\phi \approx \frac{1 - V}{2V}\left(\frac{e^{\pi\phi/2}}{1 + e^{\pi\phi}}\right) \tag{3.1}$$

which satisfies equations (2.9) and (2.10), and is suggested by the conformal mapping of the f-plane strip $0 \leqq \psi \leqq 1$ to the interior of a semi-circle of radius 1. However, the constant V in (3.1) is unknown, and so its starting value is taken to be $V \approx 1.5$.

Equation (2.9) is satisfied by imposing the conditions $\xi_1 = \frac{1}{2}\phi_1, \eta_1 = \frac{1}{2}, \eta_1' = 0$ at the first point ϕ_1 upstream, and eventually computing ξ_1' so as to satisfy the Bernoulli equation (2.7). The quantities $\eta_2, \ldots, \eta_N$ are computed from the guess at the vector $\mathbf{u}$ of unknowns using the trapezoidal rule integration formula

$$\eta_i = \eta_{i-1} + \frac{h}{2}[\eta_i' + \eta_{i-1}'] \quad i = 2, \ldots, N. \tag{3.2}$$

The downstream condition (2.10) is next satisfied approximately by defining

$$V = \frac{1}{2\eta_N}. \tag{3.3}$$

The Froude number F is now computed from equation (2.4), enabling the computation of ξ_1' at this stage.

The quantities $\xi_2', \ldots, \xi_N'$ are obtained from the approximate values of the components of the unknown vector $\mathbf{u}$ using the integro-differential equation (2.8). This equation is evaluated at the halfpoints $\phi_{k-1/2}$, $k = 2, \ldots, N$, and its domain of integration truncated to the numerical interval $\phi_1 \leqq \phi \leqq \phi_N$, using equations (2.9) and (2.10) to estimate the

contributions from the portions of the integrals which are ignored in the truncation. The integrals are discretized using the trapezoidal rule, which requires no special modification in order to cope with the singular integral on the right-hand side of equation (2.8), as pointed out by Monacella [6]. This yields a system of $N - 1$ linear equations, which can be solved for $\xi'_{k-1/2}$, $k = 2, \ldots, N$, and then $\xi'_2, \ldots, \xi'_N$ can be recovered using linear interpolation.

The values $\xi_2, \ldots, \xi_N$ are next obtained by trapezoidal-rule integration, as in equation (3.2), and then $x_2, \ldots, x_N$ and $y_2, \ldots, y_N$ are computed from (2.6). The Bernoulli equation (2.7) evaluated at the points $\phi_2, \ldots, \phi_N$ yields a non-linear system of $N - 1$ algebraic equations in the vector $\mathbf{u}$ of $N - 1$ unknowns. This system is solved by Newtonian iteration, as described by Forbes and Schwartz [4].

As a check on the numerical accuracy of our solutions, two standard internal consistency checks have been performed. The first is to establish that the results are sensibly independent of the number N of free-surface grid points, and the second is to demonstrate that the choice of ϕ_1 and ϕ_N leaves the solution unaffected. In general, it is found that the surface profiles are visually unaltered by such changes, and in each case, the values of V and F can be obtained with at least three significant figures accuracy.

4. Discussion of results

The numerical algorithm of Section 3 has been used to generate critical flow solutions for a variety of values of the semi-circle radius α. As α is increased, the speed of the downstream portion of the flow increases, with a consequent reduction in the upstream Froude number. We have been able to compute accurate solutions for values of the semi-circle radius in the interval $0 < \alpha \leqq 0.5$. For $\alpha > 0.5$, the Newton's method algorithm fails to converge, and, although the reason for this is not yet fully understood, it appears to be related to problems of numerical accuracy, rather than to any physical limitation upon the solution. This will be discussed more fully later. Solutions were computed with up to $N = 201$ free-surface grid points, as required, and all programs were run on the PYRAMID 90 XE minicomputer in the Mathematics department of the University of Queensland.

Figure 2 shows the relationship between the downstream speed V and the radius α of the disturbing semi-circle. As $\alpha \to 0$, the flow becomes more like a uniform stream with speed $V \to 1$ far downstream, but as α is made larger, the speed V increases with a corresponding decrease in the downstream fluid depth.

The variation of the upstream Froude number F with circle radius α is shown in Fig. 3. For small α, the overall flow is nearly uniform, at the critical Froude number $F \to 1$. As α is increased, the upstream Froude number decreases monotonically until the value $\alpha = 0.5$ ($F = 0.262$) is reached, at which point Newton's method ceases to converge. Figures 2 and 3 and equation (2.5) clearly indicate that the flow ahead of the obstacle is always sub-critical and behind the obstacle it is always super-critical.

Some computed non-linear free-surface profiles are displayed in Fig. 4. When $\alpha = 0.1$, there is a region of moderate curvature of the surface near the semi-circular obstruction, followed by a downstream region of uniform flow having slightly reduced depth. This qualitative description of the flow remains unchanged as α is increased, except that the variations in the surface profile become more pronounced. Thus for $\alpha = 0.5$, the surface slope becomes large near the obstruction, which is followed by a shallow uniform stream moving at high speed.

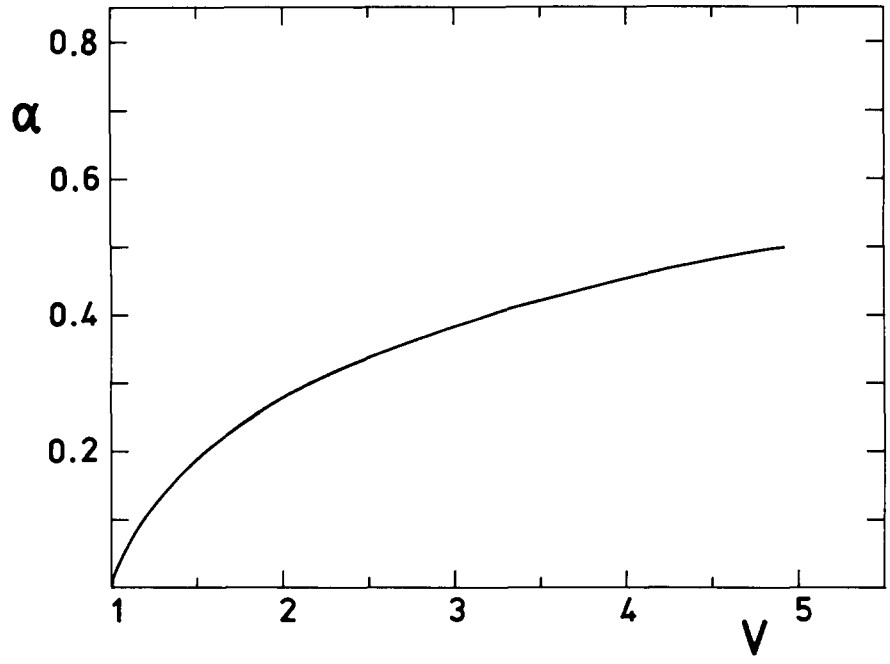

Fig. 2. Downstream speed V as a function of semi-circle radius α.

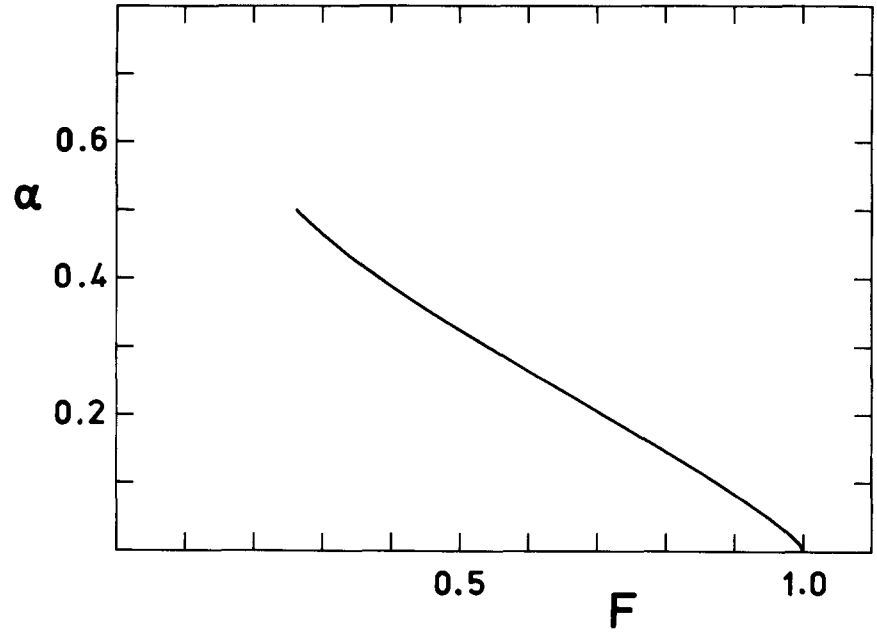

Fig. 3. Upstream Froude number F as a function of semi-circle radius α.

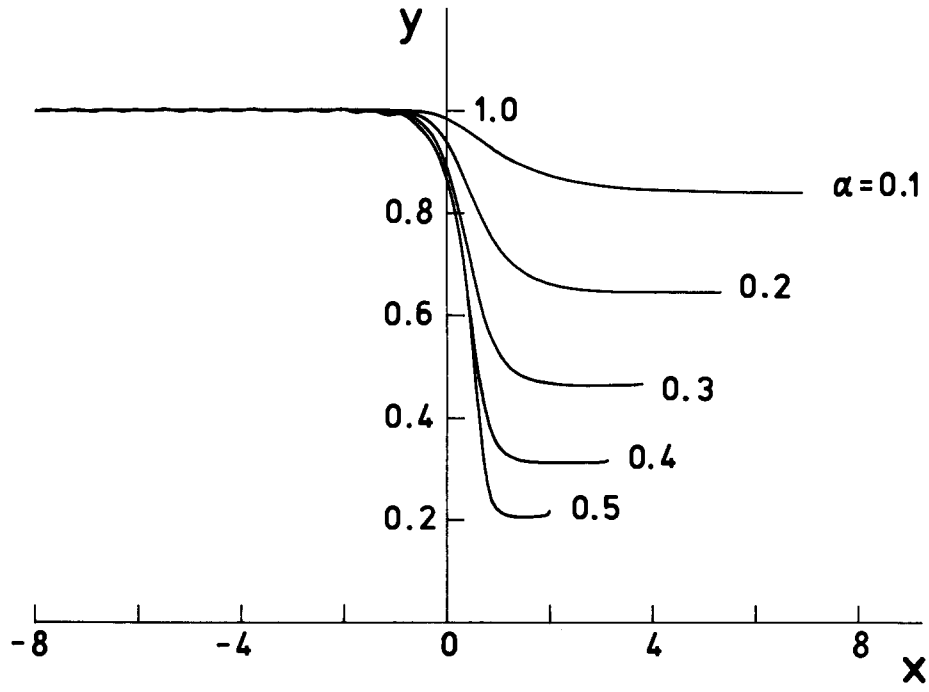

Fig. 4. Free-surface profiles obtained numerically, for five different values of α.

The solutions displayed in Fig. 4 are all of high accuracy, except the case $F = 0.5$, at which two forms of numerical error are in evidence. At this large value of α, a small, numerically-generated wave-train appears ahead of the obstacle; as explained by Forbes and Schwartz [4], these waves have no physical existence, and are a consequence of the truncation of the domain of the integro-differential equation (2.8) at the first grid-point ϕ_1 upstream. The truncation of equation (2.8) at the last point ϕ_N downstream results in an unimportant error affecting only the last few numerical grid points. This error is manifested as a small, abrupt rise in the free surface downstream, and, although slight, is visible in the profile obtained with $\alpha = 0.5$. Of far greater concern is the fact that, for large α, the downstream speed V is large, which causes the numerical grid points to cluster very close together in the downstream portion of the flow.

The failure of Newton's method to converge for $\alpha > 0.5$ can be explained in terms of the numerical errors discussed above. In particular, the clustering of numerical grid points downstream of the obstacle must ultimately erode the numerical accuracy in this region, inhibiting the ability of Newton's method to yield a solution. This problem might perhaps be overcome by using a physical-plane formulation of the problem, as in Forbes [3]. Of course, the flow becomes more singular as α increases, in the sense that the downstream portion of the flow becomes shallower and faster, and any numerical formulation must surely encounter difficulty for sufficiently large α. Indeed, the physical problem itself may become unstable at large α, since the abrupt change in bottom slope at $x = \alpha$ could cause the formation of a hydraulic jump. Thus it appears that numerical solutions may not be able to investigate the large α (small F) limit, and an alternative perturbation approach is currently under investigation.

5. Comparison with experiment

In an attempt to gauge the true effectiveness of the present numerical scheme in predicting an actual critical flow situation, the numerical results of the preceding section have been compared with results obtained from experiments performed in the Civil Engineering department at the University of Queensland. Two different semi-circular cylinders, of radii 30 mm and 75 mm respectively, were made from a cement-plaster mixture, and were successively mounted at the bottom of a horizontal rectangular flume, of width 250 mm and depth 130 mm. This apparatus is shown in Plate 1. The water depth at any point could be measured using a probe fitted with a Vernier scale, and the discharge Q in the channel could be inferred by measuring the time taken for a known mass of water to exit the flume.

Figure 5 shows a comparison of the numerical results with the values determined by experiment. The dimensionless semi-circle radius α appears on the horizontal axis, and on the vertical axis is plotted the ratio of the downstream fluid depth H_{DS} to the upstream depth H, using dimensional variables as at the beginning of Section 2. Notice that the numerical results in Fig. 5 are deduced easily from the quantity V, since the theoretical value of the ratio H_{DS}/H is simply V^{-1}.

When the semi-circular cylinder of radius $R = 30$ mm was introduced into the flume, the upstream and downstream water depths H and H_{DS} could be measured directly using the probe, and the results are shown in Fig. 5. The dimensionless ratio $\alpha = R/H$ could be varied by increasing the discharge Q, since this causes the upstream water level H to rise. With the larger cylinder of radius $R = 75$ mm, the downstream depth H_{DS} usually could not be measured reliably, since the flow downstream is fast and the water shallow, giving large relative errors in measurement. Consequently, for the larger semi-circle having $R = 75$ mm, the downstream depth H_{DS} was computed from the discharge

$$Q = cHW,$$

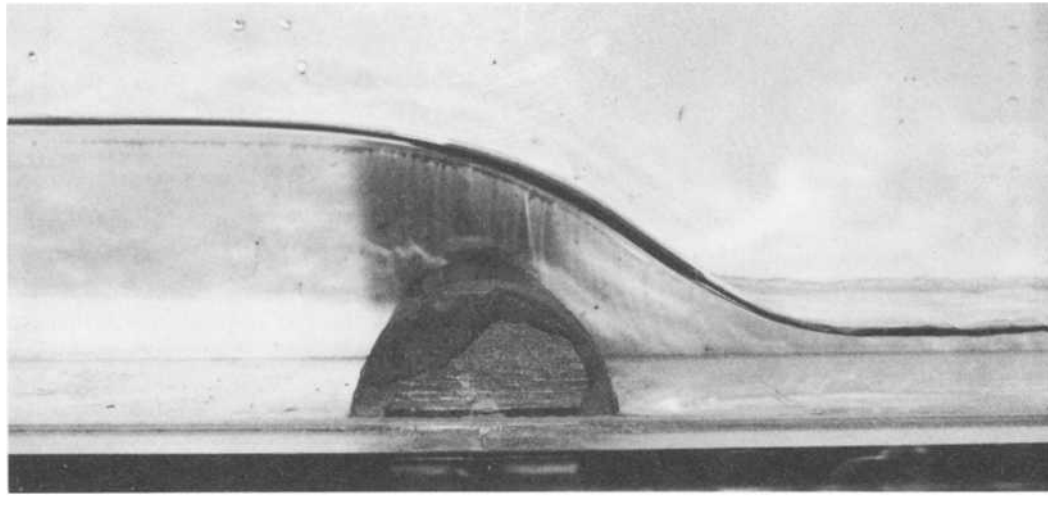

Plate 1. Experimentally observed flow over a semi-circular obstruction, of radius $R = 30$ mm. The flow is from left to right.

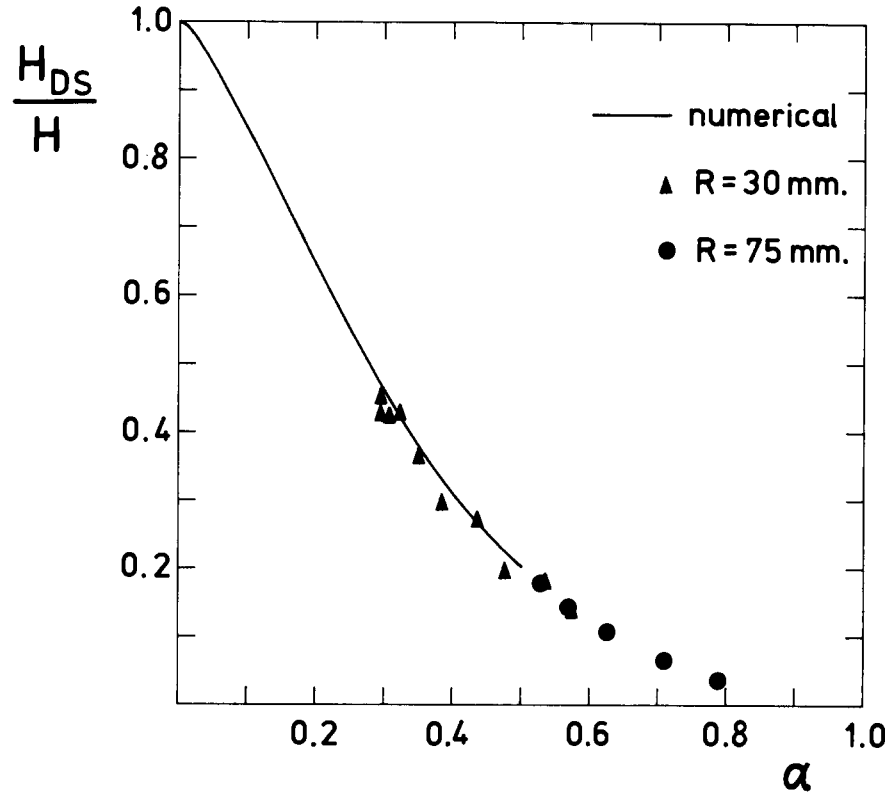

Fig. 5. The non-dimensionalized downstream flow depth, H_{DS}/H as a function of α, computed numerically and measured experimentally.

in which $W = 250\,\text{mm}$ is the channel width. Since Q and H could be measured, the velocity c could then be calculated, enabling the determination of the Froude number $F = c(gH)^{-1/2}$. The quantity V could then be obtained from equation (2.4), and its inverse finally gives the desired ratio H_{DS}/H.

From Fig. 5 it may be seen that reasonable agreement exists between the calculated and measured values, in particular when the scatter of the experimentally determined points is taken into account. Of course, the actual flow possesses effects not allowed for in the present theoretical model, such as the growth of boundary layers and fluid re-circulation near the points at which the cylinder meets the bottom of the flume. This latter effect could be observed by injecting dye into the flow, and perhaps indicates that a better comparison with experiment might be obtained for a different bottom shape in which slope discontinuities are eliminated, such as that considered by Sivakumaran et al. [8]. Nevertheless, agreement here is acceptable, and the results obtained with the larger cylinder ($R = 75\,\text{mm}$) indicate a plausible continuation of the theoretical curve in Fig. 5.

6. Acknowledgements

I am grateful to Dr J.M. Aitchison for sending a copy of her report to me in 1979, drawing my attention to the existence of critical flow solutions. Assistance with the implementation

of computer programs on the PYRAMID computer has been provided by Mr J. Zornig of the Mathematics Department at the University of Queensland, and is gratefully acknowledged. The experiments were performed, with the generous permission of the Department of Civil Engineering, in the Hydraulics Laboratory at the University of Queensland, and it is a pleasure to acknowledge the kind assistance of Dr L.T. Isaacs and the laboratory staff.

References

1. J.M. Aitchison, A variable finite element method for the calculation of flow over a weir, *Rutherford Laboratory report No. RL-79-069* (1979).
2. P. Bettess and J.A. Bettess, Analysis of free surface flows using isoparametric finite elements, *Int. Journal for Num. Meth. in Engin.* 19 (1983) 1675–1689.
3. L.K. Forbes, A numerical method for non-linear flow about a submerged hydrofoil, *J. Engin. Maths.* 19 (1985) 329–339.
4. L.K. Forbes and L.W. Schwartz, Free-surface flow over a semi-circular obstruction, *J. Fluid Mech.* 114 (1982) 299–314.
5. H. Lamb, *Hydrodynamics*, 6th edn. Dover Publications, New York (1945).
6. V.J. Monacella, On ignoring the singularity in the numerical evaluation of Cauchy Principal Value integrals, *Hydromechanics Laboratory research and development report no. 2356, David Taylor Model Basin, Washington D.C.* (1967).
7. P.M. Naghdi and L. Vongsarnpigoon, The downstream flow beyond an obstacle, *J. Fluid Mech.* 162 (1986) 223–236.
8. N.S. Sivakumaran, T. Tingsanchali and R.J. Hosking, Steady shallow flow over curved beds, *J. Fluid Mech.* 128 (1983) 469–487.
9. J.-M. Vanden-Broeck, Free surface flow over an obstruction in a channel, submitted to *Phys. Fluids.*